Design methodology to develop an active optics system for a thin 1-m meniscus mirror

Christian Schwaer[a,*] **Andreas Sinn,**[a] **Philipp Keller,**[b] **and Georg Schitter**[a]
[a]Automation and Control Institute, TU Wien, Vienna, Austria
[b]ASA Astrosysteme GmbH, Kefermarkt, Austria

Abstract. We investigate the design of an active support system for the thin primary mirror of a mid-sized telescope system used for optical satellite communication and space debris observation. To handle the complexity of this task, a general design methodology is proposed. The design for the axial and lateral support is separated into several subtasks to reduce the number of design variables in every design step. Due to the independence of mirror geometry and material, this methodology is also applicable to larger mirrors. Utilizing the proposed procedure, an active support for a 1-m meniscus mirror with 25 mm thickness and the requirement to achieve diffraction-limited optical performance is developed. The final system consists of 32 axial and 8 lateral actuators supporting the mirror with a maximal simulated RMS error of 8.8 nm and PV error of 48.0 nm when pointing to zenith. Simulations show that the obtained design ensures the required performance even under commonly occurring mirror deformations.
 [DOI: 10.1117/1.JATIS.6.4.049002]

Keywords: active optics; telescopes; mirrors; lightweight design; finite element analysis; mechatronic system design.

Paper 20096 received Jul. 1, 2020; accepted for publication Nov. 19, 2020; published online Dec. 2, 2020.

1 Introduction

High-performance telescope systems are used in a wide range of applications such as optical satellite communication,[1] satellite laser ranging,[2] and observation of space debris.[3] These applications require at least seeing limited imaging quality of the telescope systems.[4] Originally, telescopes were mainly utilized for astronomical purposes, which led to steadily increasing mirror diameters,[5] concluding with the construction of the E-ELT with a primary mirror diameter of 39 m.[6] The telescopes applied in the above-mentioned research fields are typically in the 1-m class, depending on factors such as targeted orbits, data rate, and optical resolution.[4] Furthermore, quantity, cost efficiency, and mobility are key parameters for the establishment of optical ground station networks or space debris observation collaborations, resulting in smaller, compact telescope systems. This includes, for example, NASA's 1 m Optical Communications Telescope Laboratory[7] and NICT's IN-orbit and Networked Optical Ground Stations Experimental Verification Advanced Testbed (INNOVA) with three 1-m telescopes and one 1.5-m telescope for optical satellite communication,[8] ESA's 1-m Optical Ground Station (OGS)[9] for communication and space debris detection, NASA's 1.3-m Meter-Class Autonomous Telescope (MCAT)[10] for space debris research and the 1-m Accurate Ranging system for Geodetic Observation Fixed (ARGO-F)[11] for satellite laser ranging.

The primary mirrors of these stations are manufactured with sufficient thickness to resist deformation due to gravitational load. For example, the primary mirror of NASA's 1.3 m MCAT has an approximate thickness of 130 mm, which gives it an aspect ratio of 10.[12] However, this measure leads to a large mass of the mirror and consequently large mass and higher cost of the telescope system since those evolve linearly with the primary mirror thickness.[13] Also, the thermal time constant of the mirror increases, therefore placing the telescope system within a

*Address all correspondence to Christian Schwaer, schwaer@acin.tuwien.ac.at

2329-4124/2020/$28.00 © 2020 SPIE

controlled facility may be obligated. As a result, the telescope and surrounding infrastructure lead to major investment costs.[14] Also, the local weather effects such as rain, fog, and clouds can degrade the performance of these systems. Since a network of optical ground stations is one way to overcome these limitations of optical satellite communication and space debris observation,[1] there is a need for lightweight, autonomous, and robust telescope systems.

In order to allow the reduction of the mirror mass without compromising the aperture size and maintaining the robustness toward environmental influences, large astronomical telescopes use so-called active optics, first developed for the New Technology Telescope (NTT) of the ESO.[15] This approach of an active support structure, especially for the primary mirror, allows a large reduction of mirror mass since actuators at the mirror's back are able to compensate for angle-dependent gravitational deflection of the thinner and more flexible mirror. The smaller thickness leads to a lower thermal time constant, thus decreasing temperature-dependent imaging quality. In addition, time, energy, and cost of mirror production are decreased significantly because less low thermal expansion material is consumed. Also, the requirements regarding surface shape after polishing are eased since the manufacturing error can be actively compensated.[16] Furthermore, the effort of maintaining the telescope is greatly decreased since it can use the implemented sensors and actuators to maintain itself.[15]

There are several telescopes used for astronomical purposes that implemented active optics systems after the NTT. The lightweight primary mirrors applied in these telescopes are either meniscus or honeycomb mirrors. However, the manufacturing of the honeycomb structure is more complex and expensive.[17] While there are some telescopes with meniscus mirrors above 4 m in diameter,[18–23] only few active optics systems have been reported in smaller telescopes, e.g. the 2.6-m VST,[24] the 2.1-m San Pedro Martir,[25] and the 1.0-m SONG,[26] where the latter two are not pure meniscus but flat back mirrors. Also, to prove the concept of active optics a prototype was built where the 3.6-m meniscus mirror of the NTT was downscaled to 1 m in diameter. However, the lateral support was not considered in this prototype since the mirror axis was always vertical.[27,28]

There are excellent descriptions on the design of active optics systems for large telescopes present in the literature.[15,29] However, the requirements imposed on a telescope utilized for the mentioned applications are quite different from the ones on large telescopes for astronomy. The possibly large number of telescopes with varying diameters, mirror materials, and optical designs and therefore different active support systems demand an engineering design process, which enables quick and reliable trade-off decisions regarding the mirror and support design parameters.

The main contribution of this paper is to propose a guideline for the engineering design of an active optics system for the application in telescopes of the meter-class to build lightweight, robust, cost efficient but high-performance telescope systems to satisfy the demands of current and future applications such as satellite communication and space debris observation. Active optics enables the utilization of very thin primary mirrors, significantly reducing the mass of the telescope system while maintaining robustness against environmental influences and guaranteeing high imaging performance. To the best of the author's knowledge, this is the first time the design of an active support is executed in a systematic manner with respect to the requirements demanded from a 1-m telescope system.

The paper is organized as follows. Section 2 provides a brief description of the primary mirror system. The axial support design as well as the validation of the used finite element (FE) model is presented in Sec. 3. In Sec. 4 the lateral support system is investigated. Section 5 presents the performance estimation of the developed system. Finally, the conclusion and outlook are provided in Sec. 6.

2 System Description

The active support system for the primary mirror inside the telescope is commonly separated into an axial and a lateral support system as shown in Fig. 1. The primary mirror system consists of the mirror cell as a mechanical structure to incorporate the actuators, the actuators themselves, and the primary mirror. This system is located inside a telescope system, see Fig. 2. Also

Published version of the article: Christian Schwaer, Andreas Sinn, Philipp Keller, and Georg Schitter, "Design methodology to develop an active optics system for a thin 1-m meniscus mirror", *Journal of Astronomical Telescopes, Instruments, and Systems*, Vol. 6(4) 2020. DOI: 10.1117/1.JATIS.6.4.049002

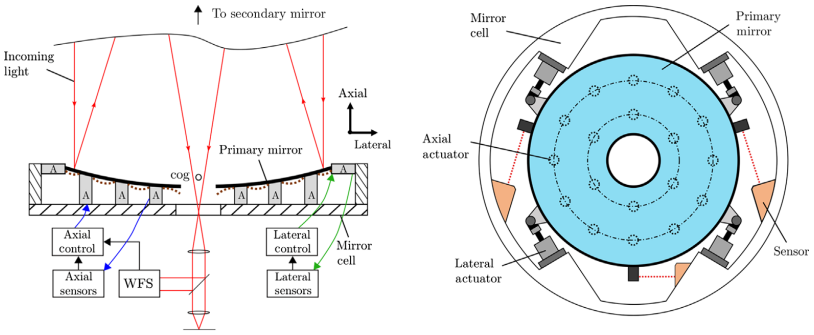

Fig. 1 (a) Layout of the primary mirror cell with active optics support. Axial and lateral supports are controlled by separate control loops, which determine the command signals for the actuators (A). (b) Front view of the mirror displaying the lateral actuators.

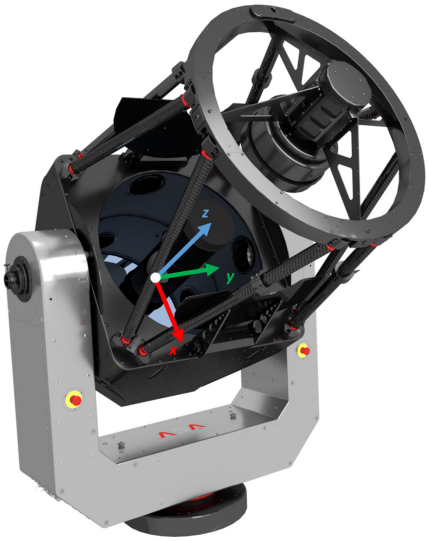

Fig. 2 Exemplary 0.8-m telescope system (AZ800) of ASA Astrosysteme.

depicted is the coordinate system used throughout this paper with the origin located at the primary's vertex, the z axis coinciding with the optical axis, the y axis coinciding with the mechanical elevation angle, and the x axis determined by the right-hand rule.

The lateral support system as shown in Fig. 1(b) ensures the position in the xy plane, whereas the axial support system keeps the position in z and the tip/tilt component around x and y, respectively. In addition, the axial actuators are used to control the mirror shape, thus incorporating the ability to compensate for environmental influences that deflect the mirror surface, such as gravity, temperature, or friction as well as shape inaccuracies after polishing. With a force sensor at each actuator to control the applied force field for the use of minimum energy modes[30] and six position sensors distributed in the mirror cell to measure all six DOFs, the actuators can be controlled to compensate for errors that influence the mirror shape as well as errors impacting the mirror position. This is achieved by applying lateral forces to move the mirror in the xy plane

Published version of the article: Christian Schwaer, Andreas Sinn, Philipp Keller, and Georg Schitter, "Design methodology to develop an active optics system for a thin 1-m meniscus mirror", *Journal of Astronomical Telescopes, Instruments, and Systems*, Vol. 6(4) 2020. DOI: 10.1117/1.JATIS.6.4.049002

Table 1 Material parameters of borosilicate glass and mirror properties.

Parameter	Symbol	Value	Unit
Density	ρ	2.23	$g \cdot cm^{-3}$
Young's modulus	E	63	GPa
Thermal expansion	α	$3.3 \cdot 10^{-6}$	K^{-1}
Poisson's ratio	ν	0.20	—
Mass	m	40.353	kg
Outer diameter	D	1.0	m
Hole diameter	d_h	0.28	m
Thickness	h	0.025	m
Radius of curvature	R_C	4.0	m

and specific force distributions axially such that the mirror surface deforms and the whole mirror holds its position through exerted piston and tip/tilt modes.[22] Although the active optics system presented in this paper is planned to be operated in open-loop after calibration using look-up tables to compensate for repeatable, gravitational effects, a wavefront sensor is added to the system in large astronomical telescopes,[15] where as of yet all active optics have been implemented, see Fig. 1(a). This way, also nonrepeatable errors on the wavefront are captured during operation and are compensated in closed-loop operation.

A complete active optics system also implements an actuated secondary mirror since misalignment with respect to the primary mirror causes aberrations, leading to image degradation. The correct alignment is important especially for wide-field telescopes[31] as often used in space debris observation.[32] However, the secondary mirror is neglected here since this paper is solely concerned about the active primary mirror support.

The primary mirror itself is typically made of borosilicate glass, fused silica, ultralow expansion glass or the glass-ceramic Zerodur. Although borosilicate glass has a larger thermal expansion than the other materials, it is often used since it is formed through casting, is easily finished by polishing, has good mechanical properties, and is an economical material.[17] Usually, the mirror has a spherical, parabolic, or hyperbolic shape, depending on the kind of telescope it is used in. While an active axial support is able to control the mirror shape, the mirror also deforms under self-weight between the discrete actuator locations as shown by the dashed brown lines in Fig. 1(a). For this reason, it is necessary to design the support accurately by taking this print through effect into account to fulfill the requirements imposed on the system, in the present case diffraction-limited performance.

The proposed design methodology can be applied to any meniscus geometry or material. In this paper, an exemplary mirror with an outer diameter of 1 m, based on the apertures of existing OGSs, with a central hole of 0.28 m and constant thickness of 25 mm is used. With a mass of around 40 kg, there is the prospect of building the whole telescope system with a mass of <500 kg.[13] The mirror data as well as the material parameters are depicted in Table 1. The telescope into which the primary mirror is integrated is a Ritchey–Chrétien f/6 with Nasmyth focus.

3 Mirror Modeling and Axial Support Design

The axial supports in active optics systems are usually located in concentric rings at the mirror back[29] since this measure reduces the number of design variables greatly with only small performance degradation as compared to optimizing every support point.[33] The axial support design is a delicate process since a thin meniscus mirror is quite compliant parallel to the optical axis. It is assumed that the mirror used to carry out the proposed design method needs to achieve diffraction-limited performance. Using the criterion of Maréchal,[34] the RMS deviation of the

Published version of the article: Christian Schwaer, Andreas Sinn, Philipp Keller, and Georg Schitter, "Design methodology to develop an active optics system for a thin 1-m meniscus mirror", *Journal of Astronomical Telescopes, Instruments, and Systems*, Vol. 6(4) 2020. DOI: 10.1117/1.JATIS.6.4.049002

deformed wavefront to the reference should not exceed $\lambda/14$. In addition, the peak-valley (PV) error should be below $\lambda/4$ for the whole wavefront. These limits are narrowed to account for further error sources, such as high-frequent spatial errors in the mirror surface, and are adapted to represent limits for surface deformation, i.e., $\lambda/30$ and $\lambda/10$, respectively. This corresponds to 17-nm RMS and 51-nm PV when green light in the middle of the visible spectrum is considered.

3.1 *Thin Plate Theory*

The utilization of flat circular plate deflection is a valuable estimation for the determination of the number of support rings and serves well as initial values for subsequent FEA.[13] Nelson et al.[33] determined expressions for thin plate deformation on an axial support, however, they do not include a central hole. This underestimates the support radii that yield the mirror surface deflection with minimal RMS when the mirror in fact has a central hole. For this reason, the hole is implemented using the governing equation for circular plate deflection

$$\frac{1}{r}\frac{\mathrm{d}}{\mathrm{d}r}\left\{r\frac{\mathrm{d}}{\mathrm{d}r}\left[\frac{1}{r}\frac{\mathrm{d}}{\mathrm{d}r}\left(r\frac{\mathrm{d}w}{\mathrm{d}r}\right)\right]\right\} = -\frac{q}{D}, \tag{1}$$

where w is the surface deflection and D is the flexural rigidity

$$D = \frac{Eh^3}{12(1-\nu^2)}, \tag{2}$$

with Young's modulus E, mirror thickness h, and Poisson's ratio ν. The distributed load q is determined by the mirror weight and area, i.e.,

$$q = \frac{P}{\pi(r_o^2 - r_i^2)}, \tag{3}$$

where P is the mirror weight, r_o and r_i are the outer and inner mirror radius, respectively. Substituting Eqs. (2) and (3) into Eq. (1) and integrating four times yields

$$w(r) = -\frac{Pr^4}{64\pi D(r_o^2 - r_i^2)} + C_1\frac{r^2}{4}[\ln(r) - 1] + C_2\frac{r^2}{4} + C_3\ln(r) + C_4. \tag{4}$$

Rearranging the terms, renaming the constants and normalizing the independent variable leads to

$$w(\rho) = -\frac{Pr_o^2}{8\pi D}\left\{\frac{\rho^4}{8(1-\xi^2)} + A\frac{\rho^2}{4}[\ln(\rho) - 1] + B\frac{\rho^2}{4} + C\ln(\rho) + F\right\}. \tag{5}$$

The terms within the parentheses are dimensionless and support-dependent, the first term is a scaling parameter with dimension of length.[35] The variable ρ is the normalized radius and ξ is the normalized hole radius. When the mirror is supported at a ring of radius $b = \beta r_o$, there are in total eight constants A_i, B_i, C_i, F_i and A_o, B_o, C_o, F_o for the region inside and outside the support ring to be determined. The boundary conditions are

$$w_o(\rho) = 0 \quad \text{at } \rho = 1, \tag{6}$$

$$w_i(\rho) = w_o(\rho) \quad \text{at } \rho = \beta, \tag{7}$$

$$\frac{\mathrm{d}w_i(\rho)}{\mathrm{d}\rho} = \frac{\mathrm{d}w_o(\rho)}{\mathrm{d}\rho} \quad \text{at } \rho = \beta, \tag{8}$$

$$\frac{\mathrm{d}^2w_i(\rho)}{\mathrm{d}\rho^2} = \frac{\mathrm{d}^2w_o(\rho)}{\mathrm{d}\rho^2} \quad \text{at } \rho = \beta, \tag{9}$$

Published version of the article: Christian Schwaer, Andreas Sinn, Philipp Keller, and Georg Schitter, "Design methodology to develop an active optics system for a thin 1-m meniscus mirror", *Journal of Astronomical Telescopes, Instruments, and Systems*, Vol. 6(4) 2020. DOI: 10.1117/1.JATIS.6.4.049002

$$-\frac{1}{\rho^2}\frac{\mathrm{d}w_i(\rho)}{\mathrm{d}\rho}+\frac{1}{\rho}\frac{\mathrm{d}^2w_i(\rho)}{\mathrm{d}\rho^2}+\frac{\mathrm{d}^3w_i(\rho)}{\mathrm{d}\rho^3}=0 \quad \text{at } \rho=\xi, \tag{10}$$

$$-\frac{1}{\rho^2}\frac{\mathrm{d}w_o(\rho)}{\mathrm{d}\rho}+\frac{1}{\rho}\frac{\mathrm{d}^2w_o(\rho)}{\mathrm{d}\rho^2}+\frac{\mathrm{d}^3w_o(\rho)}{\mathrm{d}\rho^3}=0 \quad \text{at } \rho=1, \tag{11}$$

$$\frac{\mathrm{d}^2w_i(\rho)}{\mathrm{d}\rho^2}+\frac{\nu}{\rho}\frac{\mathrm{d}w_i(\rho)}{\mathrm{d}\rho}=0 \quad \text{at } \rho=\xi, \tag{12}$$

$$\frac{\mathrm{d}^2w_o(\rho)}{\mathrm{d}\rho^2}+\frac{\nu}{\rho}\frac{\mathrm{d}w_o(\rho)}{\mathrm{d}\rho}=0 \quad \text{at } \rho=1. \tag{13}$$

Equations (10) and (11) ensure zero shear while Eqs. (12) and (13) ensure zero moment at the hole and the outer edge, respectively.

For the purpose of including the ability to remove spherical aberration by the support system since this aberration arises especially with mirrors made of material that has no extremely low thermal expansion coefficient such as the chosen borosilicate glass, it is required to support the mirror on at least three concentric rings.[36] Therefore, the analysis using the derived equations is started with an initial number of three rings. The aim is to find the support radii that minimize the RMS error of the surface deflection. Since Eq. (5) describes the deflection on one ring, the deflection on more than one ring is determined by superposition. The computational effort for this calculation is quite low, for this reason the whole solution space is investigated with a resolution of $\beta_{\text{res}} = 1 \cdot 10^{-4}$ which is equivalent to 0.05 mm. It is not reasonable to further decrease the resolution since it gets into the range of manufacturing and assembly tolerances. Since the RMS and PV error are 2.0 and 9.2 nm, respectively, the performance on three rings is already below the requirements. For this reason, the support design is continued using three rings. The normalized radii for minimal RMS on three support rings with a central hole are depicted in the first row of Table 3. It is notable that although the analytic expressions yield a good estimate it is still necessary to further investigate the mirror since a small deviation can significantly decrease the support performance.[33]

3.2 *Finite Element Analysis*

In order to fully define the axial support system, the location and number of supports have to be determined to meet the requirements regarding RMS and PV surface deflection under the mirror's own weight. For the FEA, the engineering software Ansys v.19.1 (Ansys Inc., Canonsburg, Pennsylvania) is used. The FE model of the mirror consists of 86,690 elements and 140,556 nodes in three layers along the mirror thickness. The determination of the axial support system is a three-step process to keep the design process simple by reducing the number of design parameters in every step, thus decreasing the complexity as well as the computational effort. In the first step, the mirror has a fixed support in axial direction on continuous rings and the aim is to find the ring radii that minimize the RMS error. These radii are used in the second step where the fixed support is replaced by applying line pressures to the mirror that hold it in equilibrium. The line pressures are adapted to achieve the same goal as in the first step. The last step consists of finding the minimum number of actuators in each ring to meet the imposed requirements. An overview of the design variables and the objective in every step is given in Table 2.

The optimization of the ring radii is executed as follows. A third degree polynomial is fitted to a radial slice of the surface deflection in a least-squares sense with the objective to minimize the standard deviation of the difference between the fitted polynomial and a flat radial slice. The slope of the polynomial at the radii is used to determine the radii for the next iteration. The optimization is terminated when the difference between old and new normalized radii $\beta_{\text{diff}} \leq 1 \cdot 10^{-4}$. For the line pressures, a second degree polynomial is used with the additional constraint that the sum of the weight fractions needs to be equal to one. The process is terminated if the weight fraction difference $\xi_{\text{diff}} \leq 1 \cdot 10^{-4}$.

Published version of the article: Christian Schwaer, Andreas Sinn, Philipp Keller, and Georg Schitter, "Design methodology to develop an active optics system for a thin 1-m meniscus mirror", *Journal of Astronomical Telescopes, Instruments, and Systems*, Vol. 6(4) 2020. DOI: 10.1117/1.JATIS.6.4.049002

Table 2 Steps to determine axial support design.

	Design parameters	Objective
First step	Ring radii	RMS minimization
Second step	Line pressures	RMS minimization
Third step	Number of supports	RMS < $\lambda/30$ and PV < $\lambda/10$

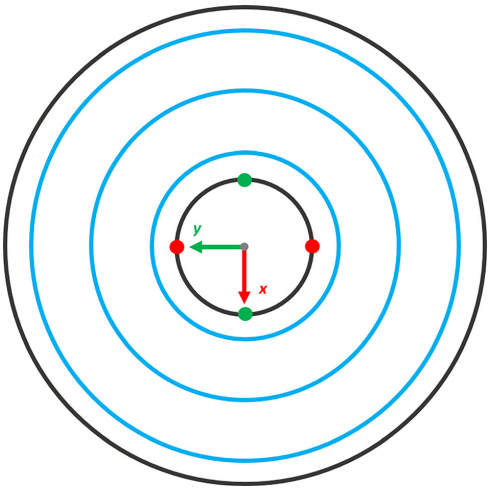

Fig. 3 Constraints in first design step. The mirror is fixed in z axis at the continuous rings (blue circles), as well as fixed in x and y at vertices of the hole (red and green dots, respectively).

Note that the axial support design is obtained for the mirror in horizontal position, i.e., pointing to zenith where the whole weight of the mirror is taken by the axial support, which is the worst case scenario.

In the first step, the ring radii obtained in Sec. 3.1 are used as initial values for the parametric FEA and are considered fixed in the direction of the optical axis z. Additional constraints are introduced to prevent rigid body motion, see Fig. 3.

A comparison between the initial FEA deflection when the mirror is supported at the radii given by the analytical solution and the deflection after the parametric FEA is given in Fig. 4(a) and the normalized support radii in the second row of Table 3. It is notable that the maximal relative error between analytical solution and FEA is 3.1%, showing the validity of the thin plate theory to determine initial values for the subsequent FEA.

In the second step, the fixed supports in the z axis are replaced by line pressures to keep the mirror in its equilibrium. To determine initial values of the line pressures, the weight fraction taken by each ring is calculated using the approximation of a flat circular plate, i.e.,

$$\xi_i = \frac{m_i}{m_{\text{mirror}}} = \frac{\rho h A_i}{\rho h A_{\text{mirror}}} = \frac{\pi(r_{m,i}^2 - r_{m,i-1}^2)}{\pi(r_{m,3}^2 - r_{m,0}^2)} = \frac{\beta_{m,i}^2 - \beta_{m,i-1}^2}{1^2 - \beta_{\text{hole}}^2}, \quad i = 1,2,3, \tag{14}$$

where $\beta_{m,i}$ is the arithmetic mean normalized radius of the i'th and $(i+1)$'th ring, and $\beta_{m,0} = \beta_{\text{hole}}$, $\beta_{m,3} = 1$. This yields the weight fractions shown in the first row of Table 4. The corresponding line pressures, which are calculated by the mirror weight and circumferences of the rings, are also displayed.

Published version of the article: Christian Schwaer, Andreas Sinn, Philipp Keller, and Georg Schitter, "Design methodology to develop an active optics system for a thin 1-m meniscus mirror", *Journal of Astronomical Telescopes, Instruments, and Systems*, Vol. 6(4) 2020. DOI: 10.1117/1.JATIS.6.4.049002

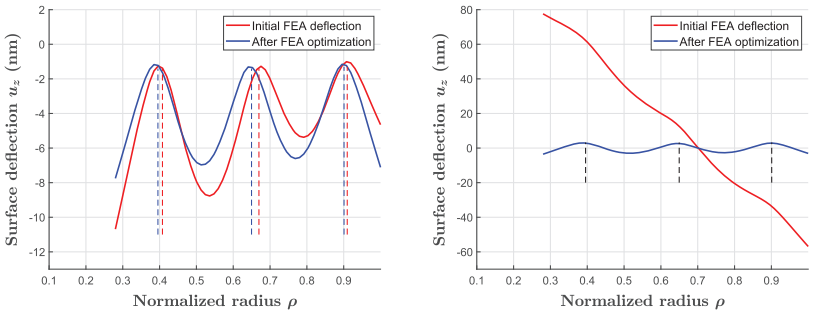

Fig. 4 (a) Comparison between initial FEA surface deflection with supports at radii given by analytical solution (red) and deflection after parametric FEA (blue). The dashed vertical lines indicate the locations of the support rings. (b) Comparison between deflection with initial line pressures (red) and deflection after parametric FEA (blue).

Table 3 Normalized ring radii determined by thin plate theory and FEA.

	β_1	β_2	β_3
Thin plate theory	0.4078	0.6698	0.9096
FEA	0.3955	0.6497	0.9009

Table 4 Weight fractions and line pressures at support rings.

	ξ_1	ξ_2	ξ_3	p_1 in N/m	p_2 in N/m	p_3 in N/m
Initial	0.2113	0.3559	0.4328	67.29	69.00	60.52
After FEA	0.2056	0.3569	0.4375	65.49	69.20	61.17

The comparison between the surface deflection before and after the line pressure optimization is shown in Fig. 4(b). It is clearly visible that the initial weight fractions determined by Eq. (14) lead to an undesirable surface deflection. After improving these as shown in the second row of Table 4, the RMS deflection is 2.0 nm and the PV is 6.5 nm, which equals the error obtained in the first design step. A comparison between the surface deflection after the first and second optimization step is shown in Fig. 5. It is obvious that the deflection is very similar after removing the piston term from the fixed support deflection. It is also notable that the analysis in Sec. 3.1 yields a good approximation for the errors to be expected after line pressure optimization, especially for the RMS error.

After determining the ring radii as well as the line pressures, the third design step consists of finding the number of supports in each ring. There are analytical investigations regarding the number and position of flat[33] and curved lightweight[35] mirrors. However, these analyses are more concerned on finding the optimal distribution of a specific number of supports than finding the support design, which achieves a necessary performance for a given mirror. Several telescopes with meniscus mirrors in various sizes that implement an active optic system choose the number of support points per ring as a multiple of three, which allows the placement of three fixed points instead of active supports at 120° (in a threefold symmetry). While this is a simple method to determine the number of supports and achieves good results,[26,37,38] it leads to uneven spacing of the support points among the rings, leaving the possibility for improvement.

Published version of the article: Christian Schwaer, Andreas Sinn, Philipp Keller, and Georg Schitter, "Design methodology to develop an active optics system for a thin 1-m meniscus mirror", *Journal of Astronomical Telescopes, Instruments, and Systems*, Vol. 6(4) 2020. DOI: 10.1117/1.JATIS.6.4.049002

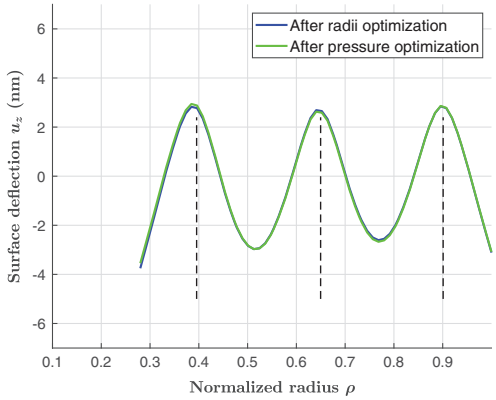

Fig. 5 Comparison between the deflection after the end of step one and step two of the FEA support design process.

The fixed points in the support with threefold symmetry are usually mechanically stiff components with sensors[29] used for position control, to take the net force and moment caused by force errors in the active support[24] or from disturbances beyond the bandwidth of the position control loop.[39] Another possibility is the use of hydraulic or pneumatic systems that are connected in sectors, thus acting as virtual fixed points.[29] However, the utilization of hydraulic or pneumatic virtual fixed points increases system complexity and replacing the active supports by real fixed points at angular separations of 120° produces a tilt for rotational symmetries other than 0 and 3.[24,29] To overcome these limitations, the use of optical sensors for the determination of piston, tip, and tilt is proposed with a position control loop that introduces stiffness by means of control to reject position disturbances on the system.[40,41] The optical position sensors and a feedback loop to the actuators enable virtual fixed points with the aim to keep the mirror position constant with respect to the mirror cell. With a sufficiently large closed-loop bandwidth, positional errors can be quickly shared across all supports[22] and the necessary balancing force field is assumed to have negligible effect on the mirror surface. Furthermore, the axial sensors can be placed where the determination of tip/tilt is most precise, i.e., at the outer edge of the mirror. Also, the effort for integration and alignment is decreased compared to physical definers.

For these reasons, the constraint of threefold symmetry is not considered during the optimization of the number of supports in each ring. To generalize the approach to obtain these, it is assumed that an azimuthal distance between the supports similar to the radial ones limits the deflection degradation to a specific degree, thus providing a good benchmark for further analysis.[37]

The radii and line pressures obtained in the first two steps are used for this analysis. It is carried out as follows:

1. The mean distance $\overline{d}_{\mathrm{rad}}$ between the three rings is calculated.
2. The number of support points is chosen such that the azimuthal distance between the points in each ring is equal to the mean radial distance

$$\zeta = \overline{d}_{\mathrm{rad}}/\overline{d}_{\mathrm{az}} \approx 1, \tag{15}$$

since the number of course has to be rounded to integers.
3. The parameter ζ is varied. The number of supports in the ring is chosen such that the azimuthal distance in each ring comes closest to the mean azimuthal distance, which is given by Eq. (15).
4. The RMS and PV deflection are obtained for several ζ and normalized by RMS and PV for the case of continuous rings.

Published version of the article: Christian Schwaer, Andreas Sinn, Philipp Keller, and Georg Schitter, "Design methodology to develop an active optics system for a thin 1-m meniscus mirror", *Journal of Astronomical Telescopes, Instruments, and Systems*, Vol. 6(4) 2020. DOI: 10.1117/1.JATIS.6.4.049002

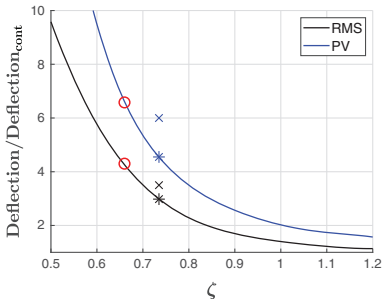

Fig. 6 Deflection degradation over ζ. The crosses show the degradation in the case of using a threefold symmetry with 6, 12, and 18 supports in three rings while the asterisks display it in the case of using a more evenly distributed design with 7, 12, and 17 supports. The red circles indicate the allowed degradation for the 1-m mirror used in this paper.

The FE model used for the analysis of the surface deflection on support points consists of forces applied to the mirror back located according to the ring radii and the number of supports per ring, which depend on ζ. The force magnitude is then determined by relating the according ring line pressure to the number of supports.

This analysis yields a relation between the displacement of the surface and deviation of azimuthal distance from radial distance. The result is shown in Fig. 6. It shows that there is a hyperbolic relation between RMS and PV deflection over ζ, where the PV degrades faster than the RMS, as is expected when a transition from continuous rings to discrete support points is performed. The crosses in Fig. 6 show the RMS and PV error of the meniscus when conventional distribution in threefold symmetry of 36 supports is used. It is clearly visible that it is beneficial when a more evenly distribution is applied, shown as asterisks.

Since the deflection is normalized by the deflection obtained on continuous rings and the number of supports in each ring is related to the ring distance, the relation shown in Fig. 6 should also be applicable to other meniscus mirrors with different geometries, materials, and number of rings. For example, the mirror shown in Ref. 13 has a similar geometry but is made of fused silica and supported by 8 and 16 points in two rings. The RMS deflection on continuous rings is 8.9 nm and PV is 31 nm. The point support design is equivalent to $\zeta = 1.12$, which yields an expected RMS of 10.7 nm and PV of 52.4 nm, whereas the FEA executed in Ref. 13 obtains 10.9 and 54 nm.

This relation is an important asset for designing a support system since the number of supports can be immediately determined after the ring support with its performance is obtained and the degradation factor is calculated with the RMS and PV requirements for the specific mirror. In the present case, with an RMS error of 2 nm and PV of 6.5 nm on continuous rings, the degradation factors to achieve diffraction-limited performance are 8.5 and 7.8, respectively. For this reason, ζ should be larger than 0.65, which yields $\overline{d}_{az} \approx 194$ mm and therefore, dividing the sum of the three ring circumferences by $\overline{d}_{az}$, 32 support points with 6, 11, and 15 supports from inner to outer ring, see red circles in Fig. 6.

The simulation result of the deflection on the 32 point support is shown in Fig. 7. The resulting RMS error of the displacement is 8.7 nm and the PV error is 42.4 nm. As also done in the analysis conducted above, the first actuator in each ring is located on the positive x axis for simplicity. The investigation of this additional DOF is beyond the scope of this paper.

3.3 *Model Validation*

To show the validity of the utilized FE model, the simulation result of an 800-mm flat back mirror is compared to interferometric measurements. The interferometer operates at a wavelength of $\lambda = 633$ nm. The mirror and support specifications are shown in Table 5.

Published version of the article: Christian Schwaer, Andreas Sinn, Philipp Keller, and Georg Schitter, "Design methodology to develop an active optics system for a thin 1-m meniscus mirror", *Journal of Astronomical Telescopes, Instruments, and Systems*, Vol. 6(4) 2020. DOI: 10.1117/1.JATIS.6.4.049002

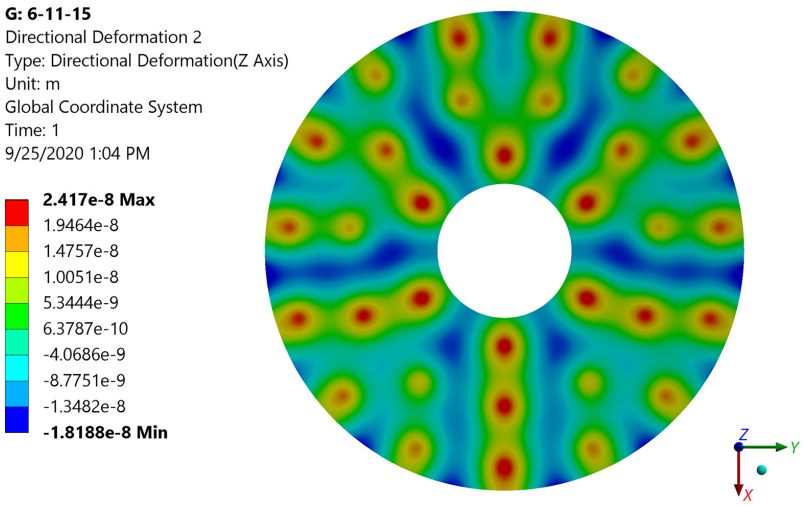

Fig. 7 Simulated surface displacement in meter on 32 support points.

After polishing, the mirror surface shape is never as perfect as the modeled one. For this reason, the measurement is executed as follows. First, the mirror is supported by three support points and the surface deformation is acquired. Second, the mirror is placed on an 18-point support and the deformation is measured again. It is assumed that the influence of an 18-point support on the surface of a mirror with the specifications shown in Table 5 is quite small, and only the modes that are polished into the mirror are visible. Afterward, the deformation on the 18 supports is subtracted from the three-point support deformation to obtain the deformation that is ideally only influenced by the support. Hereafter, the result of this subtraction is used as reference measurement data for three support points.

Table 5 Material parameters of fused silica, flat back mirror, and support data used for model validation.

Parameter	Symbol	Value	Unit
Density	ρ	2.2	$g \cdot cm^{-3}$
Young's modulus	E	74	GPa
Poisson's ratio	ν	0.17	—
Mass	m	82.16	kg
Outer diameter	d_o	825	mm
Hole diameter	d_i	231	mm
Edge thickness	h	86	mm
Radius of curvature	R_C	3994	mm
Number of supports	N_S	3	—
Support diameter	d_S	504.3	mm
Angular spacing	θ_S	120	deg

Published version of the article: Christian Schwaer, Andreas Sinn, Philipp Keller, and Georg Schitter, "Design methodology to develop an active optics system for a thin 1-m meniscus mirror", *Journal of Astronomical Telescopes, Instruments, and Systems*, Vol. 6(4) 2020. DOI: 10.1117/1.JATIS.6.4.049002

The interferometric measurement is acquired with a spatial sampling of 1.6 mm, and the FE model is adapted to have approximately the same spatial sampling at the mirror surface. The obtained data from measurement and simulation are imported to MATLAB where the Zernike coefficients of the first 80 circular Zernike polynomials[42] are determined by fitting it to the data in a least-squares-sense. The RMS error between the original and the fitted surface is calculated with

$$\mathrm{RMS}_{\mathrm{fit}} = \sqrt{\frac{1}{N}\sum_{i=1}^{N}(S_i - \hat{S}_i)^2}, \tag{16}$$

which yields 5.0 nm for the measurement and 2.6 nm for the simulation. The reason for the larger fitting error in the case of the measurement are high spatial frequency deformations in the mirror surface. Although it was tried to subtract the deformations that are inherent to the mirror surface, there is still a remaining influence if a finite number of support points is used. A plot of the difference between the raw measurement data and the Zernike fit is shown in Fig. 8, showing these deformations with high spatial frequency.

The obtained Zernike coefficients for measurement and simulation are shown in Fig. 9. Note that the large difference in defocus, i.e., mode 4, exists because defocus is always indeterminate in interferometric measurements due to the dependence on the interferometer focus. This mode was already removed during measurement and has to subtracted from the simulation data to make them comparable. In addition, piston (mode 0) that arises from the FE model constraints also needs to be subtracted from the simulation data for comparability. There is also a vertical trefoil (mode 6) present in the measurement, which is not expected for a three-point support. The raw data of the deformation on the three-point support also show this mode with approximately the same Zernike coefficient and are therefore assumed to stem from placing the mirror not perfectly centric on the support. For this reason, this mode is also removed for the next steps.

In the following, the Zernike fits of measurement and simulation are considered. Figure 10 shows a comparison of the measured and simulated data. In Fig. 10(a), the surface fit to the measurement is displayed. The fit to the FEA data with removed piston, defocus, and vertical trefoil is shown in Fig. 10(b). The difference between measurement and simulation with an RMS error of 10.9 nm is shown in Fig. 10(c).

Besides the already mentioned modes, there are other modes in the real mirror that are captured by the Zernike fit, e.g., astigmatism (mode 5) as well as modes 17 and 18 as shown in Fig. 9 that are not present in the simulation. The astigmatism mode, which is most easily excited in meniscus mirrors as shown in Sec. 5.2, is also visible in Fig. 10(c) and might originate in small

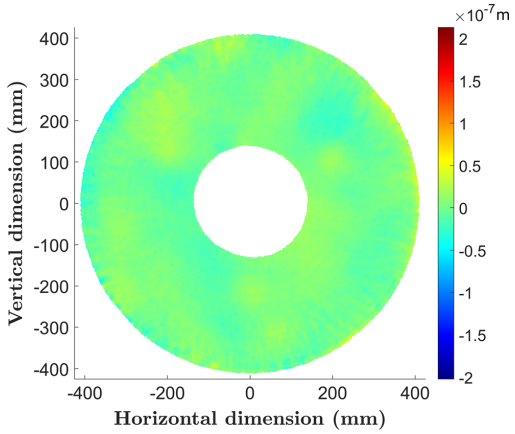

Fig. 8 Difference of surface deformation between measurement data and corresponding Zernike fit.

Published version of the article: Christian Schwaer, Andreas Sinn, Philipp Keller, and Georg Schitter, "Design methodology to develop an active optics system for a thin 1-m meniscus mirror", *Journal of Astronomical Telescopes, Instruments, and Systems*, Vol. 6(4) 2020. DOI: 10.1117/1.JATIS.6.4.049002

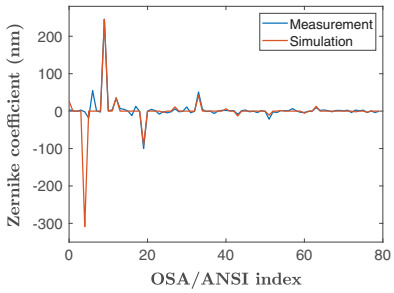

Fig. 9 Zernike coefficients for the measured and simulated data. Note that defocus (mode 4) was already removed during measurement because of the dependence on the interferometer focus.

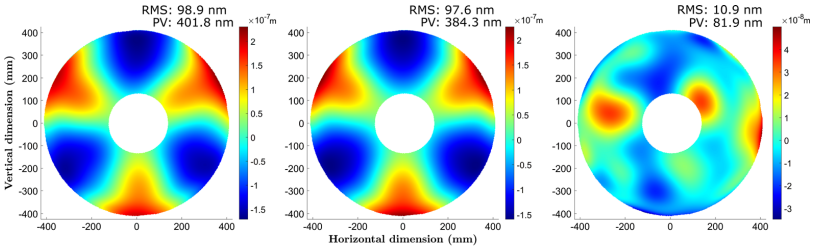

Fig. 10 Comparison between measurement and simulation. (a) Zernike fit to interferometer measurement data. (b) Zernike fit to FEA simulation. (c) Difference between measurement and simulation.

force imbalances of the support structure. The higher order modes might also stem from the asymmetry in the support as assumed for the large difference at the mirror hole and from fitting to the imperfectly removed higher spatial frequencies as shown in Fig. 8. This is especially visible in the differences at the outer edge where only a part of the polishing head covers the mirror surface.

In conclusion, an RMS error of 10.9 nm (81.9 PV) demonstrates sufficient agreement between simulation and measurement, showing that the utilized FE model can be safely applied for designing the mirror support.

4 Lateral Support Design

The former sections deal with the axial support design based on the mirror pointing to zenith. As soon as the gravity vector does not coincide with the optical axis anymore, a part of the mirror weight needs to be taken by lateral forces.

As with the axial support, the lateral support is designed for the worst case scenario: with the mirror pointing to horizon. Schwesinger[43] investigated a lateral support for meniscus mirrors depending on a parameter γ with

$$\gamma = \frac{F_t}{F_r + F_t}, \tag{17}$$

where F_r and F_t are the radial and tangential forces, respectively. The parameter γ therefore gives the contribution of tangential shearing forces to the weight support, i.e., it determines the amplitude and angle of the lateral force vectors depending on the azimuthal angle of the force application point counted from the direction of the x axis in Fig. 7. While telescopes built in the 1970s

Published version of the article: Christian Schwaer, Andreas Sinn, Philipp Keller, and Georg Schitter, "Design methodology to develop an active optics system for a thin 1-m meniscus mirror", *Journal of Astronomical Telescopes, Instruments, and Systems*, Vol. 6(4) 2020. DOI: 10.1117/1.JATIS.6.4.049002

and early 1980s such as the 4-m KPNO and the MPG/ESO 2.2 m telescope implement the special case $\gamma = 0$,[43] i.e., the mirror is supported only by forces normal to the mirror edge, the first telescope with active optics has a lateral support with $\gamma = 0.5$.[44] Since γ has a large influence on the surface deflection caused by the lateral support[45] and it was shown that supports with $\gamma > 0.5$ can be beneficial for minimizing surface deflection, more recently built telescopes[18,21,37] have varying values of γ, depending on the mirror geometry. Also, the values of $\gamma > 0.8$ are considered to be beyond the useful range.[43]

An important issue to consider when supporting thin meniscus mirrors laterally is the resulting moment that arises if the mirror cannot be supported under its center of gravity as soon as it leaves zenith position (c.f. difference between point of lateral force application and center of gravity in Fig. 1). It is usually counteracted by axial forces in cosine distribution at the mirror edge to maintain the meniscus mirror in its static equilibrium.[43]

In order to investigate the impact of the support number and the parameter γ on the surface deflection, a parametric FEA is executed. The FE mirror model is the same as used for the axial support design. A mechanical component was added to satisfy the need for an interface, which enables the application of lateral push-pull forces that are not orthogonal to the outer mirror edge. In the simulation, the mechanical component is bonded to the mirror edge since it is going to be glued to the glass mirror. The FEs of these interfaces are given a maximum edge length of 5 mm, which yields an element number of 907 with 1798 nodes. A force applied to one of the interfaces is shown in Fig. 11. As a starting point, the lower limit of the number of supports is chosen such that the stress induced by supporting the mirror with $\gamma = 0.5$ is below the limit of the material, in this case six supports. They are distributed with equal angular distance at the mid-edge of the mirror, although there are investigations with varying application point along the edge, which can extend the proposed methodology for extremely high-performance mirrors.[45,46] Then, γ is varied with a resolution of $\gamma_{res} = 10^{-2}$ to minimize the RMS deflection. This analysis is repeated several times with the number of supports increased by two after every iteration.

The value of γ for minimal RMS over the number of supports as well as the factor of improvement related to the standard support with $\gamma = 0.5$ are shown in Fig. 12. It is visible that γ is almost independent of the number of supports, the small deviation between different support numbers can be explained by the rather coarse resolution. This offers a great possibility for the

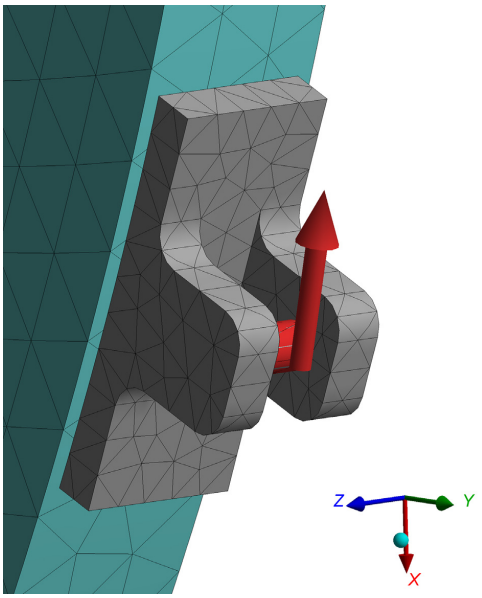

Fig. 11 Force applied to the mechanical component bonded to the outer mirror edge.

Published version of the article: Christian Schwaer, Andreas Sinn, Philipp Keller, and Georg Schitter, "Design methodology to develop an active optics system for a thin 1-m meniscus mirror", *Journal of Astronomical Telescopes, Instruments, and Systems*, Vol. 6(4) 2020. DOI: 10.1117/1.JATIS.6.4.049002

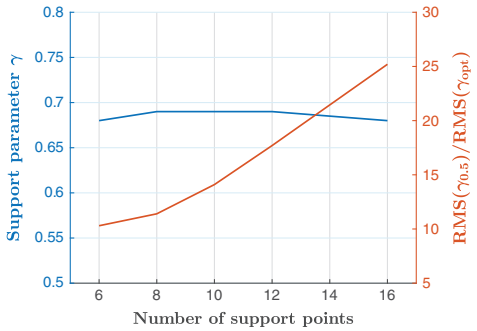

Fig. 12 Support parameter γ and RMS improvement related to standard lateral support design over the number of support points.

design approach: γ can be found by analyzing the surface deflection on a small number of supports and can then be kept constant while increasing the number of supports until the requirements are met. Further improvements can then be achieved by varying γ with better resolution around the previously obtained value. Note that γ strongly relates to the forces applied to the mirror, therefore the resolution needs to be chosen such that the support is able to provide those.

A further observation is that designs with larger numbers of support points benefit more when γ is increased, which is an important factor for designing mirrors with high imaging requirements.

When determining the number of lateral supports, two additional considerations other than RMS and PV error have to be taken into account. First, the analysis is executed in the worst case scenario when the telescope is pointing to horizon while the usual operation is up to a zenith angle of 75° or 15° above horizon, respectively. Second, the PVq ($Q = 99\%$) error is considered, i.e., 1% of the sampling points containing the largest values are neglected since the maximum deformations right at the mirror edge do not significantly contribute to overall introduction of aberrations. In the present case, the meniscus mirror is already sufficiently supported by eight lateral supports with an RMS error of 2.5 nm, a PVq error of 21.0 nm, and $\gamma = 0.70$ where γ was obtained for a number of six supports, making use of the relation shown in Fig. 12.

The support is further improved by analyzing γ around the former obtained value with a resolution of $\gamma_{\text{res}} = 2 \cdot 10^{-3}$. For comparison, the corresponding force change in direction collinear to the gravity vector is $F_{\Delta x} \approx 0.14$ N. This analysis yields an RMS deviation of 2.3 nm and PVq error of 21.3 nm for $\gamma = 0.704$. The force application points and directions of the designed support and the surface deflection are shown in Fig. 13. It is clearly visible that the largest deflections occur on a small area at the mirror edge where the forces are applied. The mechanical component interfacing the mirror and the support force is made of aluminum.

5 Performance Estimation of Complete Support

The support designed in Secs. 3 and 4 is able to passively support the mirror in its extreme angles, i.e., pointing to zenith and horizon, respectively. When the telescope is positioned at an angle in between, lateral and axial support have to work together to maintain the mirror in its equilibrium. Furthermore, the axial support is investigated regarding its ability to compensate for errors that induce surface deformations.

5.1 *Passive Support*

In order to predict the possible performance of the obtained active support, the mirror's angle with respect to the gravity vector is varied. The initial step is with the mirror pointing to zenith, afterward the zenith angle θ_z is increased by steps of 15° while the axial and lateral support forces are adapted by $\cos(\theta_z)$ and $\sin(\theta_z)$, respectively.

Published version of the article: Christian Schwaer, Andreas Sinn, Philipp Keller, and Georg Schitter, "Design methodology to develop an active optics system for a thin 1-m meniscus mirror", *Journal of Astronomical Telescopes, Instruments, and Systems*, Vol. 6(4) 2020. DOI: 10.1117/1.JATIS.6.4.049002

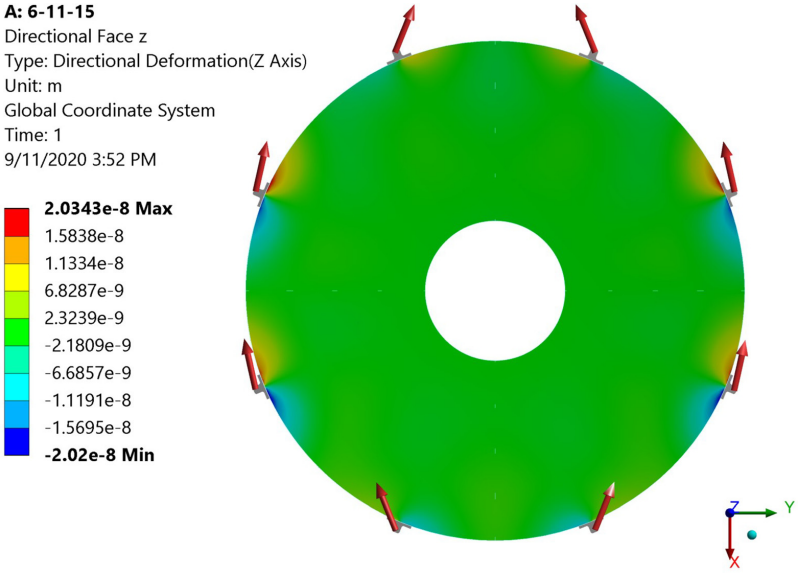

Fig. 13 The obtained lateral force directions in the *xy* plane and the resulting surface displacement when pointing to horizon.

The results of the deflection depending on θ_z are shown in Table 6. It clearly shows that the largest errors occur when the mirror's total weight is taken by the axial supports due to its compliance parallel to the optical axis and the deformations concentrating at the edge in a smaller area with increasing zenith angle. Note that the RMS error for $\theta_z = 0$ is slightly larger than stated in Sec. 3.2 due to the additional weight of the mechanical components for the lateral actuators. The PV error increases to 48.0 nm when pointing to zenith, which is still within the requirement.

5.2 *Active Support*

In order to obtain the combination of forces that yield any desired surface deformation, the effect of each actuator on the mirror figure, the influence function of this actuator, needs to be determined. The problem can then be described as

$$\mathbf{Af} = \mathbf{w}, \tag{18}$$

Table 6 RMS, PVq, and PV errors in nm for different zenith angles.

θ_z in deg	RMS	PVq	PV
0	8.8	38.8	48.0
15	8.6	38.5	47.3
30	7.9	36.3	47.9
45	6.6	32.1	45.2
60	5.0	27.4	42.4
75	3.3	22.9	39.6
90	2.3	21.3	40.5

Published version of the article: Christian Schwaer, Andreas Sinn, Philipp Keller, and Georg Schitter, "Design methodology to develop an active optics system for a thin 1-m meniscus mirror", *Journal of Astronomical Telescopes, Instruments, and Systems*, Vol. 6(4) 2020. DOI: 10.1117/1.JATIS.6.4.049002

where **f** is a row vector of the actuator forces, **w** is a row vector of the surface deflections, and **A** is the mapping matrix that comprises the influence functions that map the forces to deflections. Each column j of the matrix **A** gives the influence function for a unit force at actuator j.

The influence functions are determined by applying a unit force to one actuator and obtaining the resulting surface deflection.[39,47] This of course results in a net force and moment, which cause the mirror to leave its equilibrium. For this reason, the forces of all other actuators are adapted in proportion to their nominal force to cancel the net force and in proportion to their distance to the corresponding axis of rotation to cancel the net moment. Because of the mirror's small thickness and resulting print-through of the supports, the mirror surface is spatially sampled at 15 mm, which results in 16,871 rows for **A** and **w**. The force vector **f** has of course as many elements as there are axial supports, i.e., 32.

In order to solve Eq. (18) for **f**, singular value decomposition (SVD) is used.[48] In the over-determined case where the number of sampling points is larger than the number of actuators, the $M \times N$ matrix **A** can be written as

$$\mathbf{A} = \mathbf{USV}^T, \tag{19}$$

where **U** is an $M \times N$ column-orthogonal matrix, **S** is an $N \times N$ diagonal matrix containing the singular values, and **V** is an orthogonal $N \times N$ matrix. In the present case, **U** represents the orthogonal displacement vectors or bending modes, **V** is the orthogonal force vectors of the actuators, and **S** is the mode strengths that give the ratio of RMS surface deflection to RMS actuator force.[49]

The SVD offers the advantage that the modes used for the solution can be chosen freely. Ignoring some higher order bending modes with small amplitudes is often beneficial for two reasons. First, the low order bending modes are more easily excited than the higher order ones, which means their occurrence after polishing or due to force errors and misalignment is more likely. Second, the large forces required for the correction of high-order modes might leak into low-order modes.[39]

The first 16 modes except for mode 3 (defocus) of the mirror along with the denomination of the Zernike modes similar to the eigen modes[24,30] are shown in Fig. 14. Defocus is not compensated by the primary mirror support but by motion of the secondary mirror. Note that of the first 16 modes all except for modes 3 and 16 come in pairs and only one component of each pair is depicted.

The maximum RMS deformations, based on experienced values in mirror and telescope production, of each mode for the 1-m primary due to force differences between polishing and telescope support, gravity, thermo-elastic effects, alignment, and integration errors are displayed as red bars in Fig. 15. The correction capability of the support system is determined as follows. With an RMS error of 8.8 nm on the passive support, the maximum RMS error for a general deformation needs to be <14.5 nm to achieve diffraction-limited performance of 17-nm RMS. This means that the average RMS error over all 15 modes needs to be <3.7 nm. The force resolution of the actuators is set to $F_{\text{res}} = 5$ mN since this is the calibration force needed in the outer

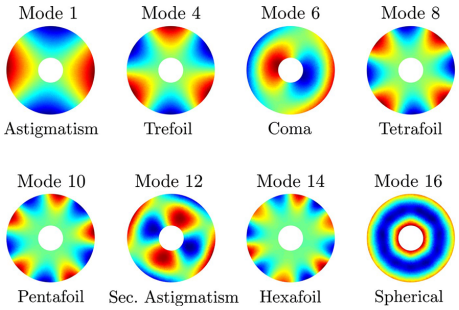

Fig. 14 Eigen modes used for active correction of the mirror. Mode 3 is compensated by motion of the secondary mirror along the optical axis. Only one component of each mode pair is shown.

Published version of the article: Christian Schwaer, Andreas Sinn, Philipp Keller, and Georg Schitter, "Design methodology to develop an active optics system for a thin 1-m meniscus mirror", *Journal of Astronomical Telescopes, Instruments, and Systems*, Vol. 6(4) 2020. DOI: 10.1117/1.JATIS.6.4.049002

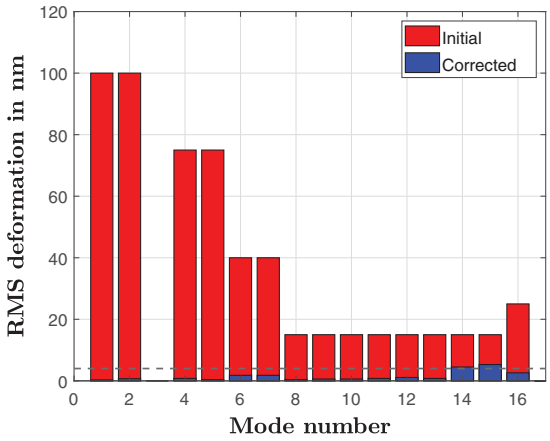

Fig. 15 The expected RMS deformations of each mode are shown as red bars, the blue bars depict the residual RMS error after actuating each mode with the axial support. The dashed line shows the residual error limit of 3.7 nm.

ring for 3.7 nm aberration coefficient in the first two modes. Based on this, the mirror is deformed in the specified modes while pointing to zenith, i.e., with the largest nominal axial forces.

The residual errors between the target modes and the corresponding eigen modes after correction of each individual mode are shown as blue bars in Fig. 15. The error in each mode is below the limit, displayed as dashed black line, except for modes 14 and 15. The azimuthal order of these modes determines the number of occurring peaks and valleys, which are coming close to the number of supports in the outer ring; therefore, a symmetry mismatch between the modes and the support system impacts the correction performance significantly. Note that the zenith-dependent deformation displayed in Fig. 7 is subtracted when determining the corrected RMS.

The correction performance of the system for a general deformation can be obtained by the performance of each mode. Therefore, the general deformation is composed of a combination of the eigen modes

$$\psi_{\text{gen}} = \sum_{k=1}^{16} \lambda_k \psi_{\text{m},k}, \tag{20}$$

where ψ_{gen} is the composed deformation, ψ_{m} is the single mode with RMS deformation specified in Fig. 15, and λ is a coefficient with a value of -1 or 1.[50]

In the worst case scenario, the mirror has to correct all modes at their maximum amplitudes in the same direction, i.e., with $\lambda = 1$ in every mode. The such-composed deformation is shown in Fig. 16(a). The simulated deformation for this case is shown in Fig. 16(b). Even in this worst case scenario, the residual RMS error is 10.9 nm and thus below the specified 14.5 nm for a general deformation as shown in Fig. 16(c). The PV error of the residual is 50.3 nm, thus also below the requirement. Note that the deformation induced by the support points is neglected in this analysis since the mirror is polished on an identical support system before transferring it into the mirror cell, thus reducing the zenith pointing surface deformation.[21]

These results verify the suitability of the proposed methodical approach to design a system for mirror support based on the seeing-limited requirements of 17-nm RMS and 51-nm PV error as well as maintaining this performance under worst-case mirror deformation of 192-nm RMS and 912-nm PV by active compensation.

Published version of the article: Christian Schwaer, Andreas Sinn, Philipp Keller, and Georg Schitter, "Design methodology to develop an active optics system for a thin 1-m meniscus mirror", *Journal of Astronomical Telescopes, Instruments, and Systems*, Vol. 6(4) 2020. DOI: 10.1117/1.JATIS.6.4.049002

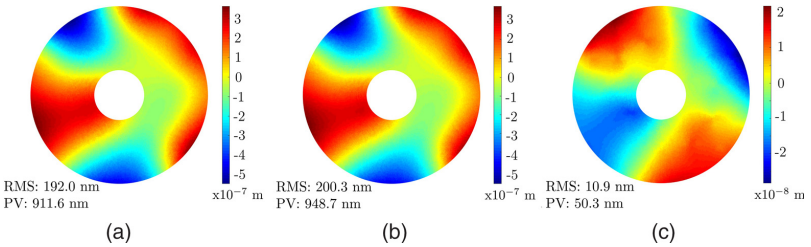

Fig. 16 Correction of a general deformation: (a) mirror deformation composed of every mode with maximum deformation. (b) Resulting mirror deformation obtained by FEA. (c) Residual error between composed deformation and simulation result.

6 Conclusion

The design of a primary mirror support system for a small telescope is proposed. This approach allows for creating an active support system for meniscus mirrors, independent from geometry or material, which makes it also applicable for larger mirrors. The design methodology is based on FEA with a single design parameter in every step to reduce computational complexity. Thin plate theory is used to obtain initial values for the subsequent FEA. The FE model consists of a floating model, which is kept in its equilibrium by axial and lateral forces. The design approach is conceived such that the minimal number of support points, and thus actuators, are obtained to meet the requirements imposed on the telescope system. An exemplary 1-m meniscus with 25 mm thickness is supported by 32 axial and eight lateral actuators to obtain a maximal RMS error of 8.8 nm and a PV error of 48.0 nm on the passive support. Further simulations show that the determined design is able to actuate the elastic modes of the mirror to compensate for commonly occurring deformations with diffraction-limited performance. To show the validity of the applied FE model, it is compared to a measurement of a 0.8-m flat back mirror with very good agreement.

The contents of this paper enable straightforward estimations on how the support changes with varying mirror thickness and material, thus enabling trade-off decisions among various parameters. For example, increasing the mirror thickness by 25%, the RMS error determined by thin plate theory is 1.3 nm. To achieve the same RMS error as on the 32-point support, the number of actuators can be decreased to 28. Decreasing the thickness by 25% gives an approximated RMS error of 3.5 nm and therefore a total number of 46 supports for the same performance. If the thickness is decreased by 50%, the calculated RMS error is 8 nm, i.e., the number of supports in each ring for the same performance as with the initial thickness has to be increased beyond the level where adding more support points significantly improves the optical quality and the addition of a fourth ring should be considered.

Building on the obtained results, future work will focus on the construction of the determined active optics system including the mirror and integrating this into a telescope system. For this, a suitable actuator to meet the requirements is currently under development with the aim to achieve high modularity. This ensures the flexible applicability to different mirrors and support designs, i.e., passive support forces and precision demands. Furthermore, the proposed methodology will be investigated regarding an additional step in the axial support design, which optimizes each actuator force to achieve even better optical performance as well as its applicability to other lightweight mirror designs such as structured honeycomb mirrors.

Acknowledgments

The authors gratefully acknowledge the cooperation with ASA Astrosysteme GmbH and thank for their support and valuable expertise. This work was funded by the Austrian research funding association (FFG) under the scope of the Austrian Space Applications Programme (ASAP), contract number 873711. The authors declare that they have no known competing financial interests or personal relationships that could have appeared to influence the work reported in this paper.

Published version of the article: Christian Schwaer, Andreas Sinn, Philipp Keller, and Georg Schitter, "Design methodology to develop an active optics system for a thin 1-m meniscus mirror", *Journal of Astronomical Telescopes, Instruments, and Systems*, Vol. 6(4) 2020. DOI: 10.1117/1.JATIS.6.4.049002

References

1. H. Kaushal and G. Kaddoum, "Optical communication in space: challenges and mitigation techniques," *IEEE Commun. Surv. Tutorials* **19**, 57–96 (2017).
2. M. Pearlman, J. Degnan, and J. Bosworth, "The international laser ranging service," *Adv. Space Res.* **30**(2), 135–143 (2002).
3. A. Potter, "Ground-based optical observations of orbital debris: a review," *Adv. Space Res.* **16**(11), 35–45 (1995).
4. H. Hemmati, A. Biswas, and I. B. Djordjevic, "Deep-space optical communications: future perspectives and applications," *Proc. IEEE* **99**, 2020–2039 (2011).
5. C. Cunningham and A. Russell, "Precision engineering for astronomy: historical origins and the future revolution in ground-based astronomy," *Philos. Trans. R. Soc. London Ser. A* **370**(1973), 3852–3886 (2012).
6. R. Gilmozzi and J. Spyromilio, "The 42m European ELT: status," *Proc. SPIE* **7012**, 701219 (2008).
7. J. M. Kovalik et al., "Optical communications telescope laboratory (OCTL) support of space to ground link demonstrations," in *13th Int. Conf. Space Oper.*, pp. 1–14 (2014).
8. M. Toyoshima et al., "Terrestrial free-space optical communications network for future airborne and satellite-based optical communications projects," in *31st AIAA Int. Commun. Satellite Syst. Conf.* (2013).
9. M. R. Garcia-Talavera et al., "Design and performance of the ESA optical ground station," *Proc. SPIE* **4635**, 38–49 (2002).
10. S. Lederer et al., "The NASA meter class autonomous telescope: Ascension Island," Tech. Rep., National Aeronautics and Space Administration (2014).
11. H.-C. Lim et al., "Technical aspects and progress of Korean SLR systems," in *18th Int. Workshop Laser Ranging* (2013).
12. S. M. Lederer et al., "NASA's orbital debris optical program: ES-MCAT updated and upgraded," in *Adv. Maui Opt. and Space Surveillance Technol. Conf.* (2019).
13. C. Schwaer, A. Sinn, and G. Schitter, "Mechatronic approach towards lightweight mirrors with active optics for telescope systems," *IFAC-PapersOnLine* **52**, 7–12 (2019).
14. K.-J. Schulz et al., "Optical link study group final report," Technical Report IOAG.T.OLSG.2012.V1, Interagency Operations Advisory Group (2012).
15. R. N. Wilson, F. Franza, and L. Noethe, "Active optics I. A system for optimizing the optical quality and reducing the costs of large telescopes," *J. Mod. Opt.* **34**(4), 485–509 (1987).
16. H. Hemmati and Y. Chen, "Active optical compensation of low-quality optical system aberrations," *Opt. Lett.* **31**(11), 1630–1632 (2006).
17. A. Ahmad, *Handbook of Optomechanical Engineering*, 2nd ed., CRC Press, Boca Raton, Florida (2017).
18. S. Guisard, L. Noethe, and J. Spyromilio, "Performance of active optics at the VLT," *Proc. SPIE* **4003**, 154–164 (2000).
19. L. Stepp, E. Huang, and M. Cho, "Gemini primary mirror support system," *Proc. SPIE* **2199**, 223–238 (1994).
20. M. Iye and K. Kodaira, "Primary mirror support system for the SUBARU telescope," *Proc. SPIE* **2199**, 762–772 (1994).
21. B. Smith et al., "The active optics system for the discovery channel telescope," *Proc. SPIE* **7739**, 77391T (2010).
22. W. Sutherland et al., "The visible and infrared survey telescope for astronomy (VISTA): design, technical overview and performance," *Astron. Astrophys.* **575**, A25 (2015).
23. V. L. Krabbendam et al., "Active optical system design for the 4.2-m SOAR telescope," *Proc. SPIE* **4003**, 122–135 (2000).
24. P. Schipani et al., "Active optics primary mirror support system for the 2.6 m VST telescope," *Appl. Opt.* **49**(8), 1234–1241 (2010).
25. L. Salas et al., "Active primary mirror support for the 2.1-m telescope at the San Pedro Mártir Observatory," *Appl. Opt.* **36**(16), 3708 (1997).
26. D. Niu, G. Wang, and B. Gu, "Active support system for 1-m SONG primary mirror," *J. Instrum.* **7**(5), T05001 (2012).

Published version of the article: Christian Schwaer, Andreas Sinn, Philipp Keller, and Georg Schitter, "Design methodology to develop an active optics system for a thin 1-m meniscus mirror", *Journal of Astronomical Telescopes, Instruments, and Systems*, Vol. 6(4) 2020. DOI: 10.1117/1.JATIS.6.4.049002

27. L. Noethe et al., "Active optics: II. Results of an experiment with a thin 1 m test mirror," *J. Mod. Opt.* **35**(9), 1427–1457 (1988).
28. R. N. Wilson et al., "Active optics: III. Final results with the 1 m test mirror and NTT 3.58 m primary in the workshop," *J. Mod. Opt.* **36**(11), 1415–1425 (1989).
29. L. Noethe, "Active optics in modern, large optical telescopes," *Prog. Opt.* **43**, 1–69 (2002).
30. L. Noethe, "Use of minimum-energy modes for modal-active optics corrections of thin meniscus mirrors," *J. Mod. Opt.* **38**(6), 1043–1066 (1991).
31. R. Holzlöhner et al., "Fast active optics control of wide-field telescopes based on science image analysis," *Proc. SPIE* **9151**, 859–873 (2014).
32. R. Sun and S.-X. Yu, "Precise measurement of the light curves for space debris with wide field of view telescope," *Astrophys. Space Sci.* **364**, 39 (2019).
33. J. R. Nelson, J. Lubliner, and T. S. Mast, "Telescope mirror supports: plate deflections on point supports," *Proc. SPIE* **0332**, 212 (1982).
34. G. Lemaitre, *Astronomical Optics and Elasticity Theory—Active Optics Methods*, Springer-Verlag, Berlin, Heidelberg (2009).
35. D.-S. Wan, J. R. P. Angel, and R. E. Parks, "Mirror deflection on multiple axial supports," *Appl. Opt.* **28**, 354–362 (1989).
36. R. Bennett and F. Baine, "Active mirror support using pneumatic actuators," *Proc. SPIE* **5497**, 91–102 (2004).
37. P. Schipani et al., "Active optics system of the VLT survey telescope," *Appl. Opt.* **55**(7), 1573–1583 (2016).
38. G. P. Lousberg et al., "Active optics system for the 4 m telescope of the Eastern Anatolia Observatory (DAG)," *Proc. SPIE* **9912**, 99126F (2016).
39. H. M. Martin et al., "Active supports and force optimization for the MMT primary mirror," *Astron. Telesc. Instrum.* **3352**, 412–423 (1998).
40. S. Ito and G. Schitter, "Atomic force microscopy capable of vibration isolation with low-stiffness z-axis actuation," *Ultramicroscopy* **186**, 9–17 (2018).
41. R. M. Schmidt, G. Schitter, and J. Van Eijk, *The Design of High Performance Mechatronics*, 2nd ed., IOS Press, Amsterdam, Netherlands (2014).
42. M. Born et al., *Principles of Optics: Electromagnetic Theory of Propagation, Interference and Diffraction of Light*, 7th ed., Cambridge University Press, Cambridge (1999).
43. G. Schwesinger, "Lateral support of very large telescope mirrors by edge forces only," *J. Mod. Opt.* **38**(8), 1507–1516 (1991).
44. G. Schwesinger, "An analytical determination of the flexure of the 3.5 m primary and 1 m test mirror of the ESO's new technology telescope for passive support and active control," *J. Mod. Opt.* **35**(7), 1117–1149 (1988).
45. G. Schwesinger, "Nondistorting lateral edge support of large telescope mirrors," *Appl. Opt.* **33**(7), 1198–1202 (1994).
46. H. Wang et al., "Multi-variable H-beta-optimization approach for the lateral support design of a wide field survey telescope," *Appl. Opt.* **55**, 8763–8769 (2016).
47. G. Parodi et al., "LBT primary mirrors: the final design of the supporting system," *Proc. SPIE* **2871**, 352–359 (1997).
48. W. H. Press et al., *Numerical Recipes: The Art of Scientific Computing*, 3rd ed., Cambridge University Press, Cambridge (2007).
49. H. M. Martin et al., "Active optics and force optimization for the first 8.4 m LBT mirror," *Proc. SPIE* **5489**, 826–837 (2004).
50. M. Laslandes et al., "Mirror actively deformed and regulated for applications in space: design and performance," *Opt. Eng.* **52**, 091803 (2013).

Christian Schwaer is a PhD student at the Automation and Control Institute (ACIN) of TU Wien. He received his MSc degree in mechanical engineering with specialization in Automation and Information Technology from Karlsruhe Institute of Technology, Germany, in 2017. His primary research interests include high performance mechatronic systems, system integration, control concepts and their application in optical systems.

Andreas Sinn is a PhD student at Automation and Control Institute (ACIN) of TU Wien. He received his MSc degree in electrical engineering from TU Wien in 2016. His primary research

Published version of the article: Christian Schwaer, Andreas Sinn, Philipp Keller, and Georg Schitter, "Design methodology to develop an active optics system for a thin 1-m meniscus mirror", *Journal of Astronomical Telescopes, Instruments, and Systems*, Vol. 6(4) 2020. DOI: 10.1117/1.JATIS.6.4.049002

interests are on high performance tip-tilt compensation systems and low-order adaptive optic systems for free-space optical (satellite) communication.

Georg Schitter is professor for Advanced Mechatronic Systems at the Automation and Control Institute (ACIN) of TU Wien. He received his MSc degree in electrical engineering from TU Graz, Austria, in 2000 and his PhD from ETH Zurich, Switzerland, in 2004. His primary research interests are on high performance mechatronic systems, scientific instrumentation and mechatronic imaging systems, such as AFM, scanning laser and LIDAR systems, telescope systems, adaptive optics, and lithography systems for semiconductor industry.

Biographies of the other authors are not available.

Published version of the article: Christian Schwaer, Andreas Sinn, Philipp Keller, and Georg Schitter, "Design methodology to develop an active optics system for a thin 1-m meniscus mirror", *Journal of Astronomical Telescopes, Instruments, and Systems*, Vol. 6(4) 2020. DOI: 10.1117/1.JATIS.6.4.049002